

## Setting Bounds on Critical Exponents with Event-by-Event Analysis of Nuclear Fragmentation Data

W. Bauer<sup>1,a</sup>, M. Kleine Berkenbusch<sup>1,b</sup>, L. Beaulieu<sup>2,c</sup>, L. Lefort<sup>2,d</sup>,  
R.G. Korteling<sup>4</sup>, K. Kwiatkowski<sup>2,e</sup>, L. Pienkowski<sup>5</sup>, S. Pratt<sup>1</sup>, A.  
Ruangma<sup>3</sup>, V.E. Viola<sup>2</sup>, and S.J. Yennello<sup>3</sup>

<sup>1</sup> National Superconducting Cyclotron Laboratory  
and Department of Physics and Astronomy  
Michigan State University  
East Lansing, MI 48824-1116, USA

<sup>2</sup> Department of Chemistry and IUCF  
Indiana University  
Bloomington, IN 47405, USA

<sup>3</sup> Department of Chemistry and Cyclotron Laboratory  
Texas A&M University, College Station, TX 77843, USA

<sup>4</sup> Department of Chemistry  
Simon Fraser University  
Burnaby, BC, Canada, V5A 1S6

<sup>5</sup> Heavy Ion Laboratory  
Warsaw University  
Warsaw, Poland

**Abstract.** An analysis of recent ISiS data [1] is performed and a comparison with percolation-based theories is conducted. We pay particular attention to detector acceptance corrections as well as the role of sequential decays of excited pre-fragments. The corrected data are subjected to a scaling analysis. We find evidence for a continuous phase transition in these nuclear multi-fragmentation events and extract the value for the critical exponents:  $\sigma = 0.5 \pm 0.1$  and  $\tau = 2.35 \pm 0.05$ . In addition, we find  $T_c = 8.3 \pm 0.2$  MeV.

*Keywords:* Fragmentation, phase transition, critical exponents, scaling analysis, percolation model, energy deposition

*PACS:* 25.70.Mn, 25.70.Pq, 24.10.Lx, 64.60.Ak, 64.60.Fr

## 1. Nuclear Fragmentation in a Three-Step Model

Multi-fragmentation reactions, in particular proton-induced multi-fragmentation reactions, can be thought of as three step processes. In the first step excitation energy is deposited and pre-equilibrium particles are emitted. In the second step the process of nuclear fragmentation takes place. Analysis of kinetic energy spectra of the fragments suggests that this process takes place at densities between roughly one-half and one-third of nuclear matter density. And in the final step, the excited pre-fragments decay via standard sequential decay channels into the fragments that can be observed in the detector.

From a many-body physics point of view the most interesting step is number two. However, step three modifies the fragment yields significantly and cannot be neglected. And extreme care has to be applied to ensure that the deposition of excitation energy is correct so that the proper set of event classes is used for step two.

### 1.1. Step Three: Sequential Decay

For step three, the sequential decay, we use a computer code recently developed by us to investigate radioactive isotope yields in RIB facilities [2]. Eight decay modes were considered: proton, neutron, deuteron, dineutron, diproton,  $t$ ,  ${}^3\text{He}$  and  $\alpha$ . The decay weights were chosen according to Weisskopf arguments. For nuclei up to Nitrogen experimentally available values were used. Decays were calculated for all levels in all nuclei, beginning with the heaviest nuclei. For the decay of each level, the decay rate was calculated into every possible level energetically accessible through the eight decay modes listed previously. The weight associated with the decaying nucleus was then apportioned into all the states in proportion to the rates for the decay into such states. The weights were also simultaneously added into the ground states of the eight nuclei representing the eight decay modes. Thus, the decaying process exactly preserved the initial  $N$  and  $Z$  of the original system.

### 1.2. Step Two: Percolation

The percolation model has been used extensively to study multi-fragmentation events [3-6]. In the variant favored by us the nucleons are represented by lattice sites, which are connected to their nearest neighbors via bonds. Expansion and thermal excitation causes the bonds to rupture, and the source to partition into fragments. The process of nearest-neighbor bond rupture is quite distinct from one based on a mean-field description or a statistical model description. Ultimately, this distinction finds its expression in the universality class (i.e. the set of critical exponents) of the phase transition, and experiments have to point the way for us to decide which model scenario is the correct one.

Here we use an approximately spherical source of a size determined by the initial pre-equilibrium emission (to be discussed in the following subsection). Transport

theory simulations of the energy deposition in proton-induced reactions support this choice of geometry [7]. For symmetric heavy ion collisions, however, this scenario may not necessarily be appropriate, and non-spherical, perhaps even non-compact [8] geometries have to be explored.

### 1.3. Step One: Energy Deposition

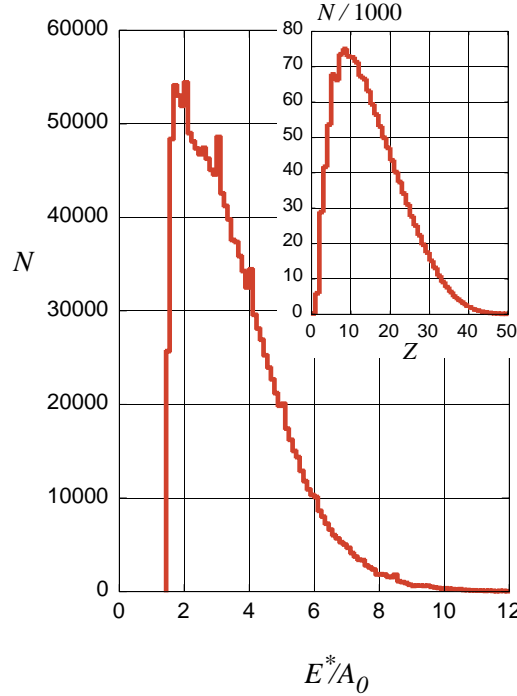


**Fig. 1.** Distribution of events as a function of deposited thermal excitation energy in the residue for the ISiS data (E900 experiment),  $p + Au$  at 10.2 GeV. The small inset shows the distribution of events as a function of total emitted pre-equilibrium charge. A total of  $1.5 \times 10^6$  events were obtained.

The percolation model of step two needs only two pieces of input, the size of the lattice and the probability with which the bonds are broken. For the size of the lattice, we use the charge of the residue after pre-equilibrium particle emission.<sup>f</sup>

The breaking probability,  $p_b$ , can be determined from the energy deposited in the system via [6]

$$p_b(E^*) = 1 - \frac{2}{\sqrt{\pi}} \Gamma\left(\frac{3}{2}, 0, \frac{B}{T(E^*)}\right) \quad (1)$$

where we utilized the generalized incomplete Gamma function  $\Gamma(x, z_0, z_1)$ ,  $B$  is the

binding energy per nucleon in the residue,  $T$  is the residue temperature, and  $E^*$  is the excitation energy per nucleon of the residue. The above formula represents a generalization of the well-know Coniglio-Klein relation [9]

$$p_{CK} = 1 - \exp(-\mathcal{E}/2T) \quad (2)$$

where  $\mathcal{E}$  is the nearest-neighbor interaction energy. Thus there is a close connection between the percolation theory and lattice gas models.

One can perform model calculations with cascade or transport programs in order to determine the energy deposition that serves as the input for the above procedure, as in [5]. Here, however, we remove the additional model dependence inherent in those energy deposition calculations and utilize, on an event-by-event basis, the energy deposition and residue size as determined by the experiment.

In figure 1 we show the experimentally determined distribution of the number of events,  $N$ , as a function of the excitation energy per nucleon of the residue. The smaller inset shows the distribution of events as a function of total emitted pre-equilibrium charge. In each event, the residue charge is then 79 minus the pre-equilibrium charge.

## 2. Inclusive Charge Yields

While the ISiS data set contains essentially complete events, it is still subject to the usual problems associated with multi-particle detector systems, such as energy cuts, gaps between the active areas of the detector elements, loss of charge- and mass-resolution for heavier fragments, and fragments that escape detection by remaining stuck in the target frame or traveling down the (typically forward section of the) beam pipe. For the quantitative study we attempt here, these effects cannot be neglected. We have thus created extensive filter software to make sure the detector acceptance effects can be accounted for.

Fig. 2 shows the comparison of our calculations with the experimental data. The data points with the (very small) error bars represent the results of the experimental charge yields. The discontinuity at charge  $Z = 17$  is due to the fact that only charges up to that value could be resolved elementally by the detector. All larger masses come from the (undetected) missing charge. The thick histogram is the result of our model calculations, as described in the previous section. Filtering our model calculations through the detector acceptance software yields the thin histogram. It is in essentially perfect agreement with the data. The discrepancy between the two histograms thus gives a good understanding of the degree to which the raw experimental data are contaminated by detector acceptance effects. For example, one can clearly see that the assumption that all undetected charges reside in one large fragment is not entirely unreasonable, but fails to reproduce the precise features of the charge yield spectrum in detail. It is at large  $E^*$  where our assumption that the missing charge is a single fragment is most likely to be in error.

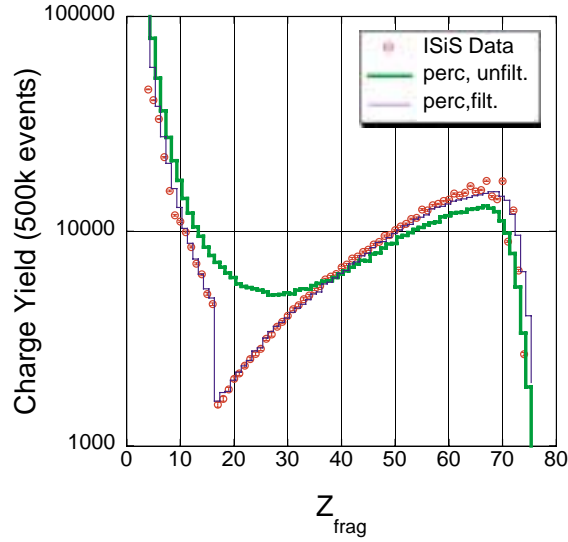


**Fig. 2.** Inclusive charge yield spectra for the reaction  $p + Au$  at 10.2 GeV. The round plot symbols represent the ISIS data, and the thick histogram is the result of the corresponding percolation model calculation. The thin histogram represents the output of passing the output of the calculation through the detector acceptance filter.

### 3. Moment Analysis

In previous studies [5] we have compared the event-by-event moments of the charge yield spectrum, binned by total charged particle multiplicity, as calculated from our model and as extracted from the experimental data of the EoS collaboration [10] and found outstanding agreement. This was interpreted as conclusive evidence for the presence of a second-order phase transition in a sub-class of the experimental data set.

The second moment of the cluster size distribution,  $n_s(p)$  (= number of clusters of size  $s$  in an event with control parameter value  $p$ ), is defined as

$$M_2(p) = \sum_s s^2 n_s(p) \propto |p - p_c|^{-\gamma} \quad (3)$$

where in the second step we have used a result from the theory of critical phenomena, thus relating the divergence of the second moment to the critical exponent  $\gamma$ . In systems with extreme finite size modifications, we cannot expect a divergence. It is even dangerous to fit any part of the  $M_2$  curve as a function of the control parameter (temperature, or otherwise) with a power-law – as shown in [5]. However, what *is* useful is a comparison between the experimental values of  $M_2$  as a function

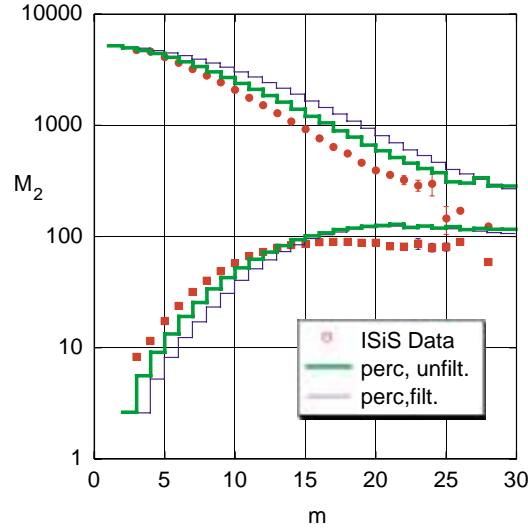


**Fig. 3.** Second moment of the charge yield distribution as a function of the charged particle multiplicity for the reaction  $p + Au$  at 10.2 GeV. Plot symbols: ISIS data, thick histogram: percolation model calculation, thin histogram: filtered calculation. The upper curves represent the case in which all fragments are allowed in the summation, and the lower curves show the result of the exclusion of the largest fragment in each individual event.

of the total charges particle multiplicity,  $m$ , with those obtained from a model that possesses both, the finite size corrections and a well-defined phase transition in the infinite-size limit. This is done in Fig. 3. One, can clearly see that the filtered calculations are quite close to the experimental data. The agreement is not perfect, partially a consequence of the assumption that all non-detected charge is accumulated in the largest fragment (as discussed in the previous section).

#### 4. Setting Bounds on the Values of the Critical Exponents

From analytical solutions and numerical results, it can be inferred that in percolation theory, for the control parameter  $p$  assuming values close to the critical value  $p_c$ , the cluster numbers behave as follows:

$$n_s(p) = s^{-\tau} f[(p - p_c)s^\sigma] \quad (\text{for } p \approx p_c) \quad (4)$$

The scaling function  $f$  has the property  $f(0) = 1$  and accounts for the fact that a power law dependence is only correct in the case of  $p = p_c$ . This must be the case because for  $p < p_c$  no system spanning cluster exists and therefore  $n_s(p)$

has to decay faster than a power law for high  $s$ .  $f(z)$  has the general form that it approaches a constant value for  $|z| \ll 1$  and decays quickly for  $|z| \gg 1$ .

Implicitly introduced by equation 4 are two critical exponents of percolation theory:  $\sigma$  and  $\tau$ . With the definition  $s_\xi = (p - p_c)^{-1/\sigma}$ , we can rewrite equation 4 as:

$$n_s(p) = s^{-\tau} f \left[ \left( \frac{s}{s_\xi} \right)^\sigma \right] \quad (5)$$

This leads to the interpretation of  $s_\xi$  as a crossover size for the cluster sizes from power law abundance for  $s \ll s_\xi$  to exponentially rare clusters of size  $s \gg s_\xi$ .

In the case of the Bethe lattice, we can give explicit terms for the scaling behavior of the cluster numbers:

$$n_s(p) \propto s^{-5/2} \exp[-((p - p_c)s^{1/2})^2] \quad (6)$$

We can immediately see the values of the critical exponents,  $\sigma = 1/2$ ,  $\tau = 5/2$  and the form of the scaling function:  $f(z) = \exp(z^2)$ .  $f$  obviously shows the asymptotic behavior mentioned before.

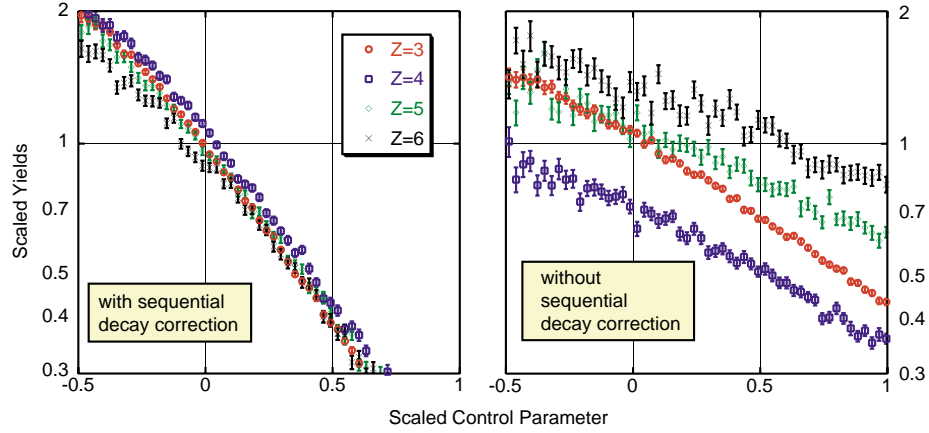


**Fig. 4.** Scaled particle yields for the  $Z = 3, 4, 5,$  and  $6$  fragments as a function of the scaled control parameter. The left-hand side shows the result of the correct inclusion of secondary decay corrections, and the right hand side shows the best fit possible when omitting these corrections.

Another special case of the general equation 4 is the scaling implied by the Fisher droplet model [11],

$$\langle n_A \rangle = \left\langle \frac{N_A}{A_0} \right\rangle = q_0 A^{-\tau} \exp \left[ \frac{A \Delta \mu}{T} - \frac{c_0 \epsilon A^\sigma}{T} \right] \quad (7)$$

One can see from this equation that when one divides both sides by the power-law term and takes the logarithm, one should expect a straight line when plotting

$\log(\langle n_Z \rangle / q_0 Z^{-\tau})$  vs.  $\epsilon Z^\sigma$  in the vicinity of the critical point, where this scaling behavior holds. In addition, the straight line should have the property of  $f(0) = 1$ . This is what Elliott et al. [12] have done recently for the EoS data as well as for the ISIS data.

However, a crucial step that was omitted in the previous work on scaling analysis is the correction for sequential decays, feeding, population of particle unstable resonances, and all other final state modifications of the charge yield spectrum. In addition, all detector acceptance corrections were neglected. We have paid particular attention to these effects in the work presented here.

How does one estimate the corrections for sequential decay on the data? There is, of course, no completely model-independent way to do this. We start with our model calculations presented in the previous section. These calculations can reproduce almost all features of the data and in particular the charge yield spectrum, after detector acceptance and final state interaction corrections. Since we know the model yields before and after the corrections, we can extract the charge-resolved correction factors. These factors are then applied to the experimental data. After that correction, we can then attempt to find a parameter set,  $\sigma$ ,  $\tau$ , and  $T_c$  that results in a collapse of all data onto a single line in the scaling analysis of the log of the scaled yield,  $\langle n_A \rangle / q_0 A^{-\tau}$ , as a function of the scaled order parameter,  $\epsilon A^\sigma$ , where  $\epsilon = (T_c - T)/T$ . The result of this  $\chi^2$  optimization procedure is shown in the left-hand-side of Fig. 4. The values for the critical parameters extracted in this way are  $\sigma = 0.5 \pm 0.1$ ,  $\tau = 2.35 \pm 0.05$ , and  $T_c = 8.3 \pm 0.2$  MeV. The contours of the  $(\sigma, \tau)$ - $\chi^2$  fit are shown in Fig. 5 for  $T_c = 8.3$  MeV.

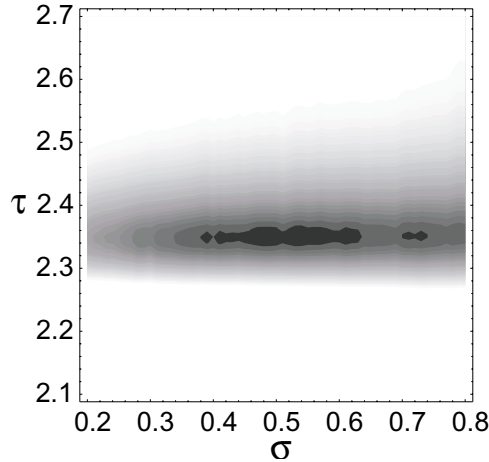


**Fig. 5.**  $\chi^2$  optimization contours for the corrected ISIS data. A value of  $T_c = 8.3$  MeV was used.

If one neglects the corrections for detector acceptance and sequential decays, then there is no way that the yields for different charges can be collapsed onto a

single scaling graph. On the right-hand-side of Fig. 4 we show the best fit result of the  $\chi^2$  optimization for that case. It is obvious that the collapse cannot be achieved.

## 5. Conclusions

We have presented a three-step model for nuclear fragmentation reactions. In order to focus on the phase transition aspects, we have elected to utilize the information on source size and excitation energy deposition provided by the experiment. For the fragmentation part of the model we use the well-known percolation approach. Particular attention is focussed on the effects of detector acceptance and sequential decays. We find that we can generate excellent agreement with the data. Since the model contains the assumption of a continuous phase transition for a certain range of excitation energies that is covered by a subset of the events in the present data set, we interpret this agreement as strong indirect evidence for a continuous phase transition.

Additional evidence for this interpretation emerges from a scaling analysis, carefully conducted to correct for the effects of sequential decay and detector resolution. We find that the data show very good scaling behavior, as expected in the vicinity of the critical point. The critical parameters extracted from a  $\chi^2$  optimization procedure have the values  $\sigma = 0.5 \pm 0.1$ ,  $\tau = 2.35 \pm 0.05$ , and  $T_c = 8.3 \pm 0.2$  MeV.

## Acknowledgement(s)

This work was supported by NSF grant PHY-0070818. MKB also received funding from the Studienstiftung des Deutschen Volkes. WB acknowledges support from an Alexander-von-Humboldt Foundation Distinguished Senior U.S. Scientist Award. The work reported on here was part of the Master's thesis of MKB.

## Notes

- a.* E-mail: bauer@pa.msu.edu  
URL: <http://www.pa.msu.edu/~bauer/>
- b.* E-mail: berkenbu@nscl.msu.edu
- c.* Present address: Département de Physique, Université Laval, Laval, Quebec, G1R 2J6 Canada
- d.* Present address: LPC, IN2P2 - CNRS, F-14050 Caen Cedex, France
- e.* Present address: Los Alamos National Laboratory, Los Alamos, NM 87545, USA
- f.* Alternatively, one could also consider to use the *mass* of the residue. For the theory this provides no difficulties whatsoever. However, in the experiment only the charges of particles are detected. Thus it is natural to use the charge as the relevant quantity in our calculations.

## References

1. T. Lefort et al., Phys. Rev. Lett. **83**, 4033 (1999); L. Beaulieu et al., Phys. Lett. **B163**, 159 (1999); L. Beaulieu et al., Phys. Rev. C **63**, 031302 (2001).
2. S. Pratt, W. Bauer, Ch. Morling, and P. Underhill, Phys. Rev. C **63** 034608 (2001); W. Bauer, S. Pratt, Ch. Morling, and P. Underhill, Heavy Ion Physics, in print (2001).
3. W. Bauer et al., Phys. Lett. **150 B**, 53 (1985); W. Bauer et al., Nucl. Phys. **A452**, 699 (1986).
4. X. Campi, J. Phys. A **19**, L917 (1986); T. Biro et al., Nucl. Phys. **A459**, 692 (1986); J. Nemeth et al., Z. Phys. A **325**, 347 (1986).
5. W. Bauer and A. Botvina, Phys. Rev. C **52**, R1760 (1995); W. Bauer and A. Botvina, Phys. Rev. C **55**, 546 (1997).
6. T. Li et al., Phys. Rev. Lett. **70**, 1924 (1993); T. Li et al., Phys. Rev. C **49**, 1630 (1994).
7. G. Wang, K. Kwiatkowski, V.E. Viola, W. Bauer, and P. Danielewicz, Phys. Rev. C, **53**, 1811 (1996).
8. W. Bauer, G.F. Bertsch, and H. Schulz, Phys. Rev. Lett. **69**, 1888 (1992); L. Phair, W. Bauer, and C.K. Gelbke, Phys. Lett. **B314**, 271 (1993).
9. A. Coniglio and Klein, J. Phys. A **13**, 2775 (1980); X. Campi, X. and H. Krivine, Nucl. Phys. A **620**, 46 (1997).
10. J.B. Elliott et al., Phys. Rev. C **49**, 3185 (1994); M.L. Gilkes et al., Phys. Rev. Lett. **73**, 1590 (1994); H.G. Ritter et al., Nucl. Phys. A **583**, 491c (1995).
11. M.E. Fisher, Physics **3**(5), 255 (1967).
12. J.B. Elliott et al., Phys. Rev. Lett. **85**, 1194 (2000); C.M. Mader et al., preprint nucl-th/0103030 (2001). J.B. Elliott et al., preprint nucl-ex/0104013 (2001).